Supplementary Information

Characterization of di-4-ANEPPS with nano-black lipid membranes

Maria Tsemperouli, Kaori Sugihara*

Department of Physical Chemistry, University of Geneva, Quai Ernest Ansermet 30, 1211 Geneva 4, Switzerland

* corresponding author: kaori.sugihara@unige.ch

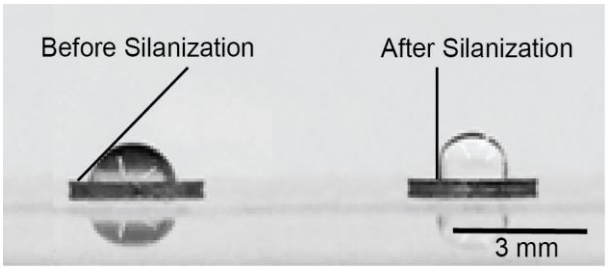

Figure S1. Contact angle measurement of Si_3N_4 chip surface before and after the hydrophobic silanization.

Contact angle measurements. The contact angle of distilled water on Si_3N_4 chip surface before and after silanization was observed to confirm the successful hydrophobic surface functionalization.

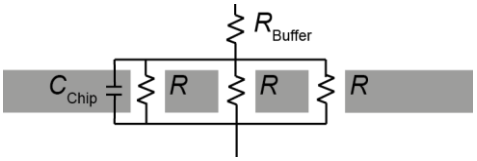

Figure S2: Schematic representation of the equivalent electrical circuit of the Si_3N_4 chip with pores.

Analysis of impedance spectra. In the main manuscript we presented the results of the estimated resistance values of each chip after fitting with an indicated equivalent circuit in Table

1. The presented chip resistance values are in the same order of magnitude as what it is theoretically expected from the dimension of the pore and the solution conductivity of the buffer solution. The resistance of the chip ($R_{Chip} = 1/G_{Chip}$: the inverse of the conductance of the chip G_{Chip}) comes from the pores, because the rest of the Si_3N_4 membrane is an insulator. Theoretically, the chip resistance (R_{Chip}) with a single pore can be estimated by:

$$R_{Chip} = \rho \cdot d/A$$

, where ρ is the solution resistivity, d is the thickness of the Si_3N_4 membrane and A is the area of the pore. In case there are N pores in the chip, the resistance from each pore will be electrically connected in parallel (see Figure S2), thus the total chip resistance R'_{Chip} will be:

$$1/R'_{Chip} = 1/R + 1/R + 1/R + \ldots = N/R$$

$$\therefore R'_{Chip} = R/N = \rho \cdot d/AN \qquad \text{(because } R = \rho \cdot d/A\text{)}$$

Therefore, the chip resistance R_{Chip} is inversely proportional to the number of the pores N. The values of R_{Chip} in Table 1 are indeed roughly scaled by $1/N$, which corresponds to the theoretical estimation.

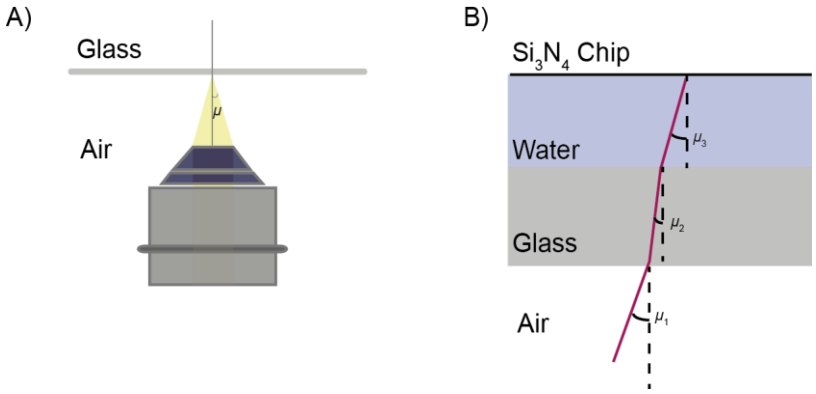

Figure S3: (A) Schematic representation of the fluorescence illumination through the objective in an inverted epifluorescent microscope. The incident light angle μ is one-half the angular aperture and is the maximum angle of light illumination that can be achieved with an objective of a given numerical aperture (NA). (B) Light pathway during fluorescence illumination of di-4-ANEPPS in lateral nano-BLM in our setup.

Analysis of light propagation and excitation of di-4-ANEPPS. A schematic representation of the illumination through the objective of an inverted epifluorescent microscope is presented in Figure S3A. The angle of the incident light is dependent on the numerical aperture (NA) of the objective lens in use and the refractive index (n) of the medium (1.0 for the air) according to the following equation:

$$\mathrm{NA} = n \sin(\mu)$$

In this work, the illumination is coming through a long distance objective lens (air objective) with 40x magnification (numerical aperture NA = 0.7). In air, the angle of the light that comes out from this objective is maximum 44 ° based on the above equation. This is the objective with the maximum NA we could use with our setup due to the restriction that comes from the spacing between the bottom glass coverslip and the Si_3N_4 membrane in the inner electrochemical chamber. Note that this value is the maximum angle (see the above scheme in Figure S3A), thus the illumination contains light with angles at 0 – 44°. In addition, this angle is modified by that fact that this illumination goes through air (1.0), glass (n = 1.52), and buffer solution (n = 1.33) to finally reach the nano-BLMs (Figure S3B). Due to the fact that it passes these different

interfaces, the final maximum incident angle that the illumination has at nano-BLMs is roughly 32°.

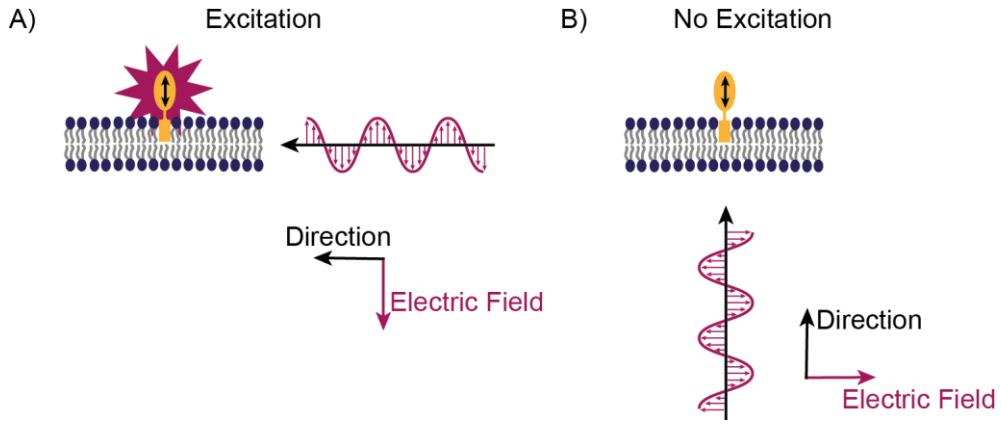

Figure S4: A scheme showing the relative orientation of dye's electronic dipole moment, the plane of lipid bilayer, and the propagating light. (A) The efficient excitation of dye molecules occurs only when the direction of electric field component of the incident light is parallel to the dye's electronic dipole moment. (B) In the lateral BLM configuration, this condition is not satisfied.

For the efficient excitation of di-4-ANEPPS the orientation of the electric field of the propagating light has to match with that of the dipole of the dye (μ has to be 90°). See Figure S4A. Since our incident light has the maximum angle of 32°, this reduces the efficiency of the excitation dramatically. Nevertheless, the fact that our illumination has an angle $\mu \neq 0$ must be a large part of the reason why we still detect some signals from di-4-ANEPPS.

The lipids in the annulus (the edge of the pores) are not in plane with the chip (see Figure 1 in the main manuscript). Therefore, di-4-ANEPPS inserted inside these lipid structures will emit much higher fluorescence. However, these di-4-ANEPPS molecules will not contribute to the voltage-dependent signals significantly, because the effective electric field E (= V/d, where V is the applied voltage, d is the thickness of the BLM) at the annulus is negligible due to the high thickness (roughly the same as the Si_3N_4 membrane, 200 nm).

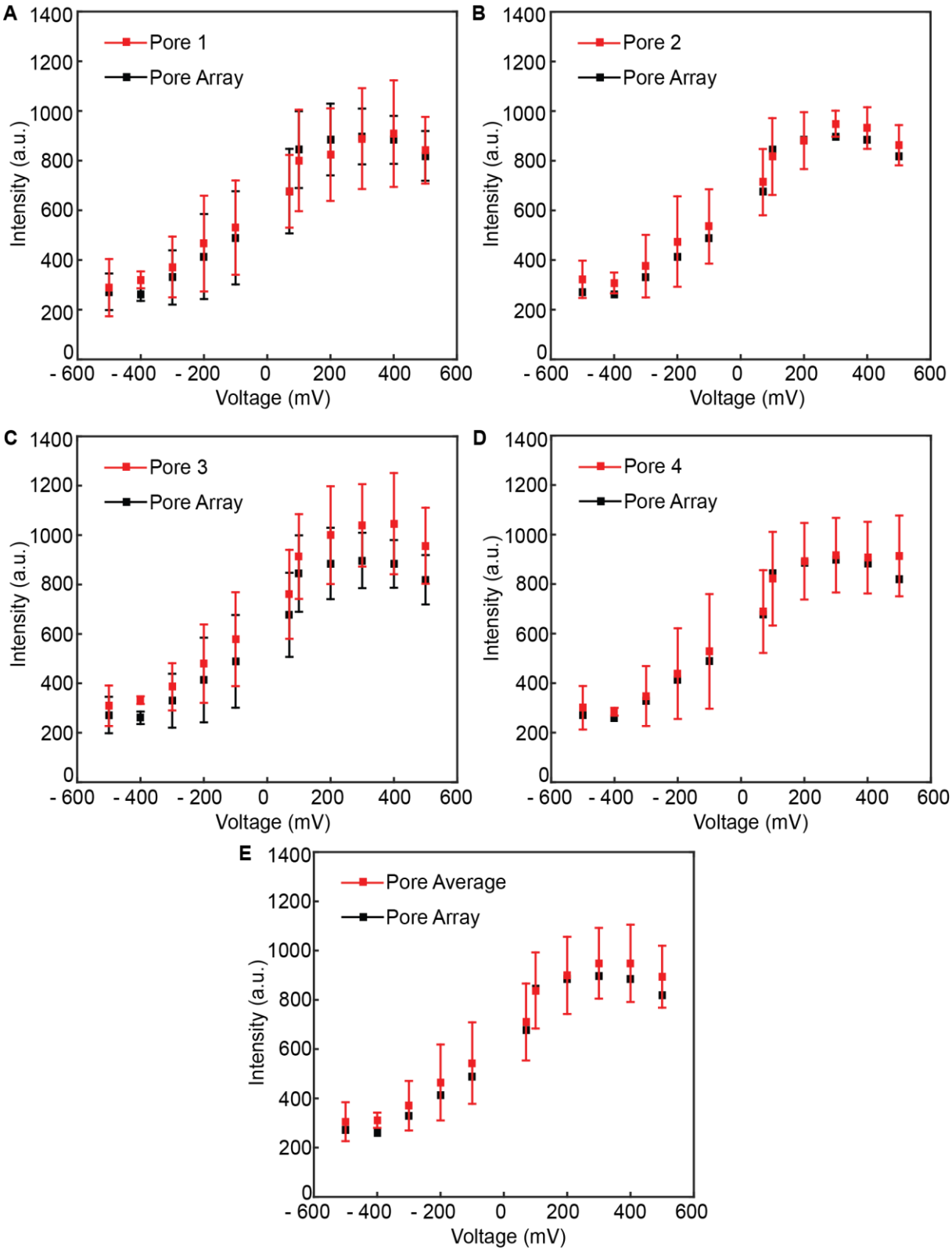

Figure S5. Comparison of di-4-ANEPPS calibration curves in POPC nano-BLMs obtained by different image analysis procedures. The analysis from the entire pore array (black line in A-D), from each individual pore (red line in A-D), and the average of the intensity from the individual pores (red line in E) were plotted.

Analysis of fluorescence signals from di-4-ANEPPS. In the main manuscript, the fluorescence intensity from the entire pore array was plotted against applied voltages for the calibration curve (Figure 7). In Figure S5, we performed a similar analysis but this time a pixel-sized area at the center of each individual pore was selected as region of interest instead of the entire pore array. These calibration curves from individual pores (red lines in Figure S5A-D) and their average (red line in Figure S5E) are all quantitatively similar to the analysis from the entire pore array (black lines in Figure S5A-E). This suggests that the voltage sensitivity of the di-4-ANEPPS in nano-BLMs is identical in each pore, which demonstrates the good reproducibility of our platform.

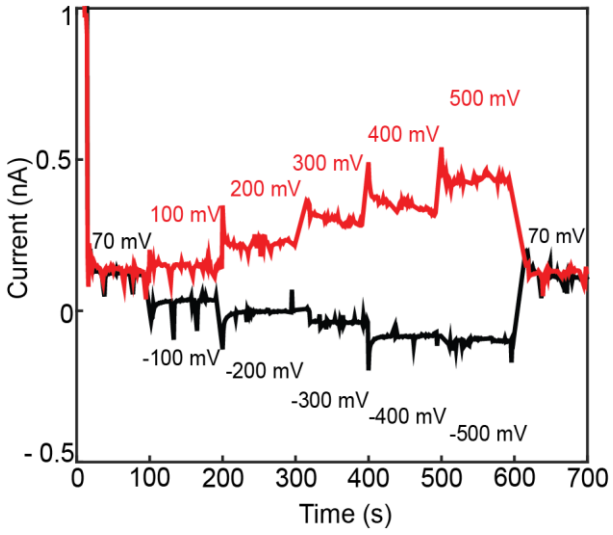

Figure S6. Typical chronoamperometric plots during voltage-dependent fluorescence imaging of di-4-ANEPPS incorporated in BLMs. Note that each time when optical microscopy imaging was performed, a noise spike appeared in the electrical signal due to the mechanical vibration for switching bright field and fluorescence mode, which we removed from the plot for simplifying the figure. Before time 0 s, 0 mV was applied to the nano-BLMs.

Current response during the voltage-dependent fluorescence signal recording of di-4-ANEPPS. In the main manuscript, to study the voltage sensitivity of di-4-ANEPPS incorporated in BLMs, different DC voltage sequences were applied by the four-electrode configuration (Figure 6). Figure S6 presents the current that was recorded over time during this

experiment. The current values altered each time when a new voltage was applied. It is because BLMs are not a perfect insulator but have a certain conductance. The measured current after saturation at each voltage is in good agreement with the one expected from the estimated BLM resistance *R* from the impedance measurement (Figure 4) and the applied voltage *V* (*I* = *V*/*R*). Capacitive currents are also present at the beginning of each applied voltage step, which indicates that ions require time to accumulate on both sides of nano-BLMs for establishing a constant membrane potential.

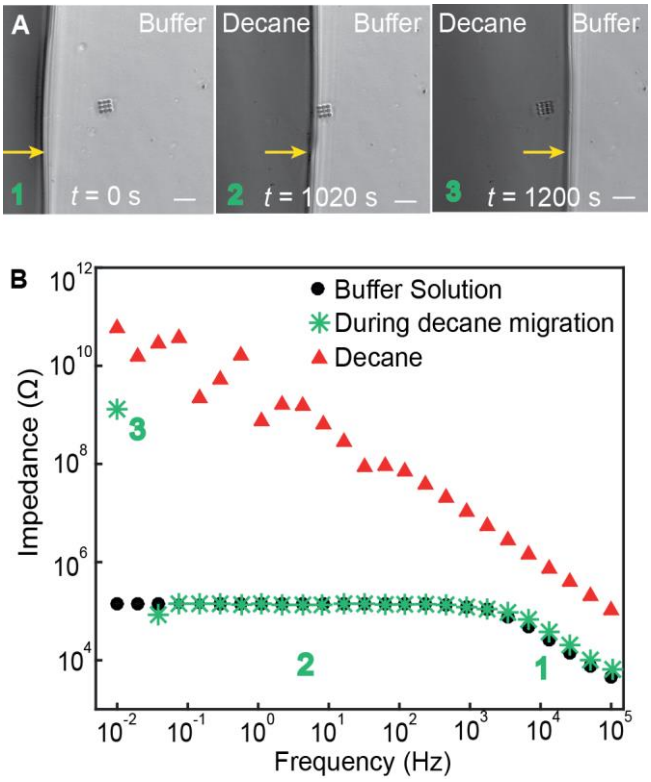

Figure S7. Optical and electrical characterization of a decane-clogged 9-pore array. (A) Bright-field microscopy images of 9-pore Si_3N_4 membrane during the migration of decane over the pore array area. The decane/buffer solution interface is indicated with a yellow arrow. (B) Impedance spectra simultaneously measured during the migration of decane on the surface.

Painting pores with decane without lipids. In the main manuscript, we presented a calibration curve from a control experiment without lipids, where di-4-ANNEPS showed no voltage-sensitivity (Figure 7). Figure S7A shows snapshots from a bright-field microscopy movie, where decane without lipids was added on chip's surface in the presence of aqueous buffer solution. Decane migrated on the hydrophobic Si_3N_4 membrane surface over time and clogged the pore array at t = 1200 s. Impedance spectroscopy was conducted simultaneously to capture this moment electrically (Figure S7B). A large increase in the impedance at low frequency (Z ≈ 10 GΩ at f = 0.01 Hz) after the coverage of the pore array by decane was observed as expected. The result shows that such impedance spectra (red in Figure S7B) can be obtained without forming BLMs but just by clogging the pore with decane. Unfortunately, the analysis of capacitance from the spectra does not provide the identity of the materials inside the pores (BLMs or just decane), because the extraction of the bilayer thickness is impossible with our system due to the too high capacitance that originates from the Si_3N_4 membrane. Therefore, the final proof for the nano-BLM formation requires the monitoring of di-4-ANEPPS response.

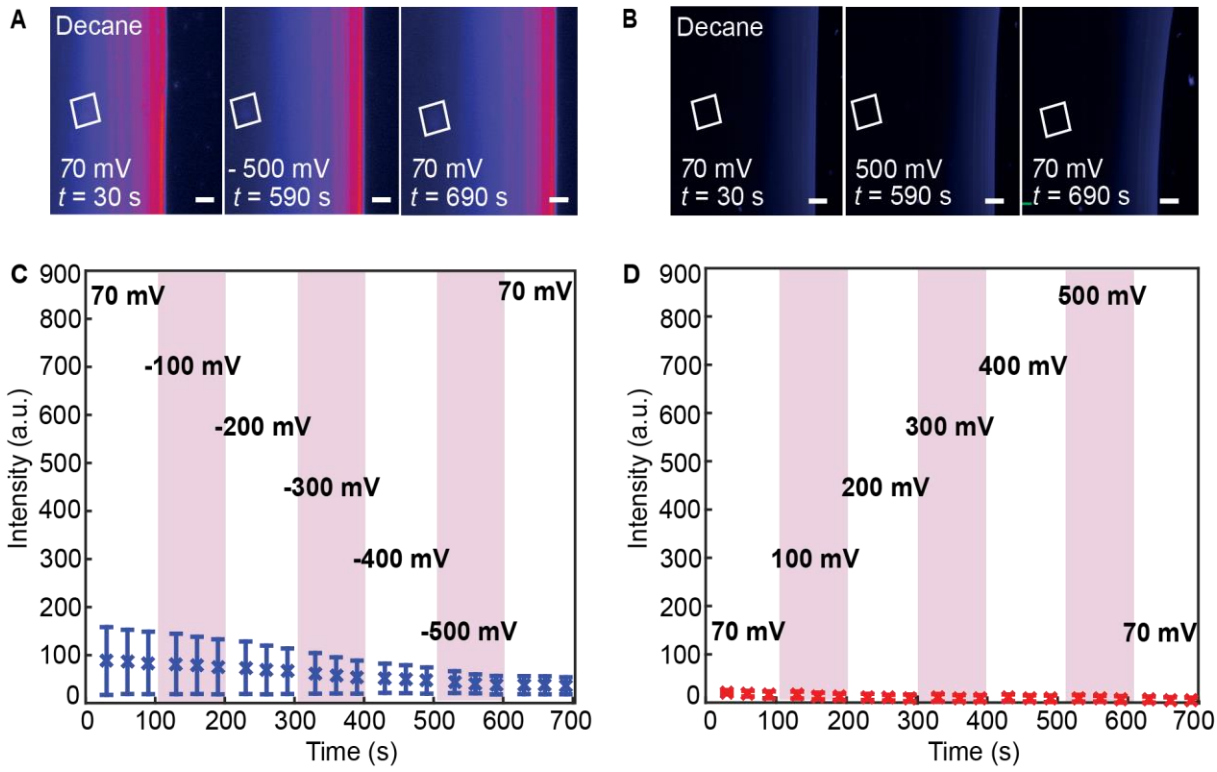

Figure S8. (A, B) Voltage-dependent fluorescent images of di-4-ANEPPS in decane-clogged 9-pore array chip (scale bar 10 μm). (C, D) Total fluorescent intensity from the pore area is plotted over time. The position of the pore array is indicated with a white square.

Following to the coverage of the pore array with decane, 200-400 μL of di-4-ANEPPS stock solution (100 μM) was added to the inner chamber at a final concentration of 10-30 μM (0.005% ethanol from the di-4-ANEPPS stock solution was present) for staining (1h incubation time). Figure S8AB shows the fluorescent images of decane-buffer interface over a 9-pore chip stained with di-4-ANEPPS at different applied membrane potentials. The location of the 9-pore array is highlighted with a square in white solid line in each image. In Figure S8CD, the total fluorescence intensity from the pore area is plotted against time, where each applied voltage is also indicated. This control experiment shows that di-4-ANEPPS presents little fluorescence and no voltage dependence. The corresponding calibration curve is shown in the main manuscript in Figure 7. The lack of voltage-dependent response is probably because of the

incorrect alignment of the dyes at the decane/water interface, where the dipole is not parallel to the applied electric field like in case of dyes in lipid membranes. In such a case, there is no efficient coupling between the external electric field and the electronic transitions of the chromophore, thus the probe does not respond to changes in the potential as it has been previously reported[1].

REFERENCES

1 E. Fluhler, V. G. Burnham and L. M. Loew, *Biochemistry*, 1985, **24**, 5749-5755.